

Characterization of ionospheric total electron content data using wavelet-based multifractal formalism

Shivam Bhardwaj^a, E. Chandrasekhar^{b,*}, Gopi K. Seemala^c, Vikram M. Gadre^a

^a Department of Electrical Engineering, IIT Bombay, Powai, Mumbai, Maharashtra, 400076, India

^b Department of Earth Sciences, IIT Bombay, Powai, Mumbai, Maharashtra, 400076, India

^c Indian Institute of Geomagnetism, New Panvel, Navi Mumbai, 418023, India

ARTICLE INFO

Article history:

Received 14 June 2019

Revised 4 January 2020

Accepted 25 January 2020

Keywords:

Magnitude cumulants of wavelet transform

Multifractal analysis

Ionospheric TEC

P-model of multiplicative cascades

ABSTRACT

Understanding of the spatio-temporal behaviour of nonlinear geophysical signals, such as ionospheric total electron content (TEC) by multifractal analysis brings out the chaotic and intermittent nature of the signal under consideration. Wavelet-based multifractal analysis was performed on TEC data and the horizontal component of the Earth's magnetic field (henceforth referred to as H-component) data recorded during geomagnetic storm events at a few sites in equatorial, mid-latitude and high latitude regions (30°S to 80°N), confined to a narrow longitude band (35°W – 80°W) (geographic coordinates) during the solar minimum (2008) and solar maximum (2014) years. The study was done using the magnitude cumulant analysis of the wavelet transform. The advantage of this technique, over the well known wavelet transform modulus maxima (WTMM) method in studying the multifractal behaviour of nonlinear signals is explained. Results show that during the major geomagnetic storm events (Dst. Index ≤ -50 nT) both TEC and the H-component data exhibit strong multifractal behavior and that the degree of multifractality (representative of the width of the multifractal spectrum) for the H-component data is more than that of TEC for all latitudes regardless of solar conditions. A nonlinear P-model, representative of multiplicative cascades for the above data sets, also supports the above observation. It has been observed that these observations hold good when multifractal behaviour of TEC data, with and without its dominant diurnal component, is compared with that of H-component data. A statistical hypothesis testing of the above results obtained using bootstrapping technique also establishes the significance level of the multifractal behaviour of the data.

© 2020 Elsevier Ltd. All rights reserved.

1. Introduction

Ionosphere is a part of the Earth's upper atmosphere, which is highly ionized and lies at an altitude ranging from 60 km to 1000 km. The main source for ionization is the solar radiation. The electron density in the ionosphere exhibits spatio-temporal variation varying as a function of latitude (space) and longitude (time) [1]. Any electromagnetic (EM) wave travelling through the ionosphere suffers a refraction which depends on the frequency of the EM wave. In particular, for an EM wave of frequency f_o , the ionosphere acts as a refractive medium with a refractive index, μ_I , defined as $\mu_I = 1 - \frac{K_1}{f_o^2}$, where $K_1 = -40.3N_e$, here N_e is the number of free electrons in the ionosphere (see <http://www.gnss.be>). Therefore, a study of spatio-temporal variation of number of electrons in

the ionosphere, as it affects satellite communication, is an area of acute research interest among geophysicists and space scientists. Also the ionospheric total electron content (TEC) is an important quantity as it facilitates to understand the behaviour of the Earth's upper atmosphere during different solar conditions. The typical TEC data show very high intermittency and non-stationarity, which suggest the highly complex and nonlinear behaviour of ionospheric dynamics. Therefore, there is a need to employ nonlinear mathematical techniques that can accurately capture these nonlinear dynamics in the underlying signals.

The electron density in the ionosphere at a given location depends usually on the solar activity like solar EUV flux, the neutral composition of the atmosphere and on the combined dynamical effect of neutral winds and electric fields [2]. During geomagnetic storms, a sufficiently intense and long lasting interplanetary convection of electric field leads to a substantial energizing of the Earth's magnetosphere. This disturbance in the interplanetary medium can be attributed to solar coronal mass ejection (CME),

* Corresponding author.

E-mail address: esekhar@iitb.ac.in (E. Chandrasekhar).

which often leads to sudden changes (usually decrease) in the H-component intensity and also in the electron density of the ionosphere [3]. Dst (abbreviation for Disturbance storm time) is an important index for studying the geomagnetic storms and related phenomena [4]. This index characterizes the intensity and nature of the geomagnetic storms [5,6]. Knowledge of the dynamic behaviour of both these nonlinear geophysical data sets recorded simultaneously, is always important.

Multifractal analysis of signals provides us with a set of measures that indicates the intermittency and chaos in the process of generating the signal [7]. The main aim of multifractal analysis is to quantify the local scaling behavior of signal under consideration. From the statistical point of view, such an analysis tells us the presence of long term or short term correlations present in the signal. In the context of signal analysis, such an approach provides a way to come up with parametric models for signals based on the exponents that are obtained from local scaling behaviour of the signals under consideration [8–10]. Various methods for multifractal analysis of signals and other multidimensional measures exist in the literature, which give more or less the same results for physical data [11–15]. For 1-D signals multifractal analysis involves local detrending of the signal in the natural domain (time, space). This is done to remove any polynomial trends that masks the singularities in the data. Popular techniques in this regard are DFA (Detrended Fluctuation Analysis) and MFDFA (Multifractal DFA) [13,14,16–18]. Another important time-frequency based method that is widely used for doing multifractal analysis is the wavelet transform modulus maxima (WTMM) method. It essentially relies on the fact that most of the useful information in the data can be retrieved by following the local maxima of wavelet transform at different scales [11,12,19,20].

Wavelets have proven to be important mathematical tools to analyze nonstationary signals because in most of the naturally occurring signals the nonstationarity arises due to the presence of the polynomial trends in the data [15,20]. The number of vanishing moments that each wavelet possess helps to remove these polynomial trends in the data, resulting in easy identification of singularities for their subsequent characterization [21]. A wavelet function having n vanishing moments, $n \in \mathbb{Z}_+$, can unmask or detrend the polynomial trends of order $n - 1$ in the data and make the data more stationary. Then, ergodicity argument can be applied to the detrended data to calculate higher order statistical moments. These statistical moments help to determine various multifractal measures that indicate the nonlinearity and chaos in the dynamics of the system that generates them [19,22].

Two well-known ways of performing wavelet analysis are: Continuous wavelet transform (CWT) and Discrete wavelet transform (DWT). CWT is employed to study the multifractal behavior of data using WTMM method [12,19,20] and magnitude cumulant analysis method [23,24]. DWT is employed to study the multifractal behaviour of the data using wavelet leaders and wavelet p-leaders [25–27]. In this paper we employ the wavelet-based nonlinear multifractal formalism, involving the magnitude cumulants of wavelet transform coefficients obtained by CWT to effectively characterize the TEC recorded during solar minimum (2008) and solar maximum (2014) years.

An important parametric model for multifractal data is popularly known as P-model of multiplicative cascades [28,29]. P-models are characterized by the value of a parameter P that can be used to quantify the degree of multifractality in the data, representative of the spectral width of a multifractal process. In this paper P-models corresponding to H-component data and TEC data of different latitudes have been identified and discussed concerning the dynamics of these multifractal processes.

The paper is organized as follows. Section 2 provides the details of the database. Section 3 briefly describes wavelet-based

multifractal formalism based on cumulants of the magnitude of wavelet transform, followed by fitting the P-model of multiplicative cascades [30] for the singularity spectrum obtained via wavelet-based multifractal formalism. Section 4 describes some results related to multifractal analysis based on the technique described in Section 3 and inspecting the statistical significance of the empirical results obtained using bootstrapping technique. Finally Section 5 provides the conclusions.

2. Data Base

For the present study, GPS data corresponding to the solar minimum (2008) and solar maximum (2014) years have been obtained from Scripps Orbit and Permanent Array Centre (SOPAC), California (see <http://sopac.ucsd.edu/dataBrowser.shtml>), where a repository of GPS data from different IGS (International GNSS Service) stations (see <http://www.igs.org/network>) is maintained. Full description of the downloaded data and the procedure to calculate TEC values from GPS data can be found in [18] (see also <http://seemala.blogspot.in/>).

The H-component data, sampled at 1 min. interval and the Dst index sampled at 1 hr. interval were downloaded from World Data Center (WDC-C2) for geomagnetism, Kyoto, Japan (<http://wdc.kugi.kyoto-u.ac.jp/index.html>) and World Data Center (WDC) for geomagnetism, Edinburgh (<http://www.wdc.bgs.ac.uk/data.html>). In the present study, we considered the TEC and the H-component data of only those days, when the Dst. index is ≤ -50 nT.

The sites corresponding to TEC and H-component data are chosen in such a way that they are located as closely as possible. Table 1 gives the list of magnetic observatories and IGS sites for TEC together with their geographic coordinates considered for the present study. Fig. 1 shows an example plot of variation of Dst. index, the H-component data recorded at a low latitude station, SJG and the TEC data recorded at the site, CRO1 corresponding to the geomagnetic storm event of March, 2008. Table 2 lists the number of geomagnetic storm events considered for analysis in the present study that correspond to 2008 and 2014 recorded at the sites given in Table 1. The TEC data considered in the present

Table 1

List of TEC and geomagnetic observatory sites, whose data were used in the present study.

S.No.	Latitude Zone	IGS (TEC) and IAGA (Mag. obs.) codes and coordinates for the sites
1.	Lower Latitude Zone	CRO1 (Lat.:17.756, Long.:−64.58) SJG (Lat.:18.117, Long.:−66.42)
2.	Middle Latitude Zone	ALGO (Lat.:45.958, Long.:−72.071) OTT (Lat.:45.403, Long.:−75.552)
3.	High Latitude Zone	QAQ1 (Lat.:60.715, Long.:−46.01) NAQ (Lat.:61.167, Long.:−45.435)

Table 2

List of geomagnetic storm events together with their respective Dst indexes corresponding to solar quiet (2008) and disturbed (2014) years. The H-component data and TEC data used in this study correspond to these dates.

S.No.	Storm Duration	Dst. Index
1.	28–29 Feb, 2008	−52 nT.
	19–20 Feb, 2014	−119nT.
2.	26–28 March, 2008	−56 nT.
	28 th Feb.–2 nd March, 2014	−52 nT.
3.	09–10 August, 2008	−57 nT
	27–29 August, 2014	−79 nT
4.	04 September, 2008	−51 nT
	12 September, 2014	−88 nT
5.	11 October, 2008	−54 nT
	14 October, 2014	−50 nT

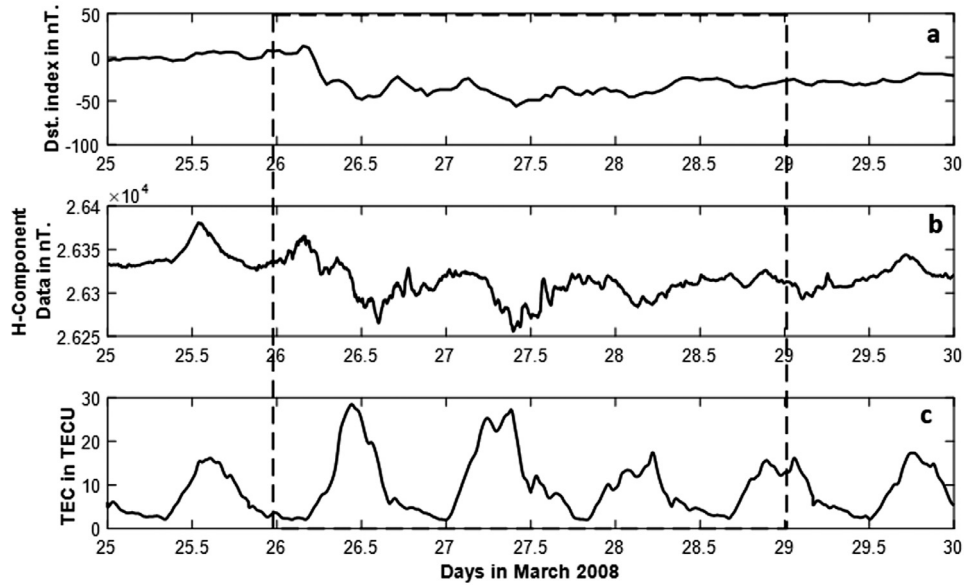


Fig. 1. Variation of (a) Dst index, (b) Horizontal component of the Earth’s magnetic field recorded at SJG and (c) TEC recorded at CRO1 (see Table 1 for site co-ordinates). Portion of the data shown in the dashed box corresponds to the geomagnetic storm event of 26–28 March, 2008.

study correspond to the same dates of geomagnetic storms shown in Table 2, but recorded at IGS sites.

3. Wavelet transform-based multifractal analysis

3.1. Multifractal formalism

Multifractal formalism is the process of extracting spectrum of singularities from a given sample path of a stochastic process. A function $f : \mathbb{R} \rightarrow \mathbb{R}$ has a local Hölder exponent $h(x_0)$ around the point x_0 if,

$$|f(x) - P_n(x - x_0)| \leq C|x - x_0|^{h(x_0)} \tag{1}$$

here, C is the proportionality constant, $h(x_0)$ is the largest real number for which the Eq. (1) holds. $P_n(x - x_0)$ is the polynomial of degree $n \in \mathbb{Z}_+$ such that $n \leq h(x_0) < n + 1$. $P_n(x - x_0)$ is the n^{th} order Taylor series approximation of the function in the neighborhood of x_0 . For example, if $2 \leq h(x_0) < 3$ then the singularity is in the second derivative of f and $P_n(x - x_0)$ is the second order Taylor series approximation of $f(x)$ in the neighborhood of x_0 . Similarly, if $0 \leq h(x_0) < 1$, then $P_n(x - x_0)$ is just the value of the function at x_0 . With the above definition intact, one can define the spectrum of singularities for a function f as $D(h)$, where $D(h)$ is the Hausdorff dimension of all the points x_0 in the domain of f , where the local singularity exponent is h . If h varies largely (remains constant) throughout the domain of f , then, such a function is called multifractal (monofractal).

An important parametric model for monofractals is given in terms of their self-similarity. According to Mandelbrot et al. [8], a process $f(t)$ is self-similar with stationary increment, τ if for $\mu > 0$ and $\mu \in \mathbb{R}$,

$$\{f(t_0 + \tau) - f(t_0)\} \approx \{\mu^{-H}[f(t_0 + \mu\tau) - f(t_0)]\} \tag{2}$$

Here, “ \approx ” indicates identity in finite dimensional distribution (Note here that $f(t)$ is treated as a stochastic process. So the value this function takes at each t is a random variable). H is called the Hurst exponent and has the same connotation as Hölder exponent in deterministic setting. The value of H lies between 0 and 1. $H > 0.5$ indicates the presence of long-range dependencies (LRD) in the data, which indicates that increasing trends in the past implies increasing trend in the future and vice-versa. $H < 0.5$

indicates the presence of short range dependence (SRD), which indicates anti-persistent behaviour in the data, suggesting increasing trends in the past implies decreasing trend in the future and vice-versa. However, $H = 0.5$ represents a complete random time series [31,32].

3.2. Wavelet-based multifractal formalism and singularity detection

In recent years, the wavelet transform has proven to be an important tool for the analysis of multifractal measures and functions [12,25,26]. Wavelets are the functions that have finite time-bandwidth product [20]. They have zero average (if $\psi(t)$ is a wavelet function then $\int_{\mathbb{R}} \psi(\tau) d\tau = 0$) and unit \mathcal{L}_2 norm, i.e, the wavelet function ψ , follows,

$$\|\psi\|_{\mathcal{L}_2}^2 = \int_{\mathbb{R}} |\psi(\tau)|^2 d\tau = 1$$

These two properties leads to the admissible condition,

$$\int_0^\infty \frac{|\hat{\psi}(\omega)|^2}{|\omega|} d\omega < \infty$$

where $\hat{\psi}$ represents the Fourier transform of ψ [33]. Wavelets turn out to be a complete orthonormal basis for the space of finite energy signals, i.e. for the set of functions in $\mathcal{L}_2(\mathbb{R}) := \{f, \forall f \in \mathcal{L}_2(\mathbb{R}), \int_{\mathbb{R}} |f(\tau)|^2 d\tau < \infty\}$. This property leads to a sparse representation of signals in the wavelet domain. For the purpose of singularity detection, non-orthogonal decomposition of signals (or functions) in terms of wavelets of varying scale is proven to be useful and is commonly referred to as continuous wavelet transform (CWT) in literature [34,35], i.e. for a function $f \in \mathcal{L}_2(\mathbb{R})$ the CWT is given by:

$$WT_f(u, s) = \langle f, \psi_{u,s} \rangle = \int_{\mathbb{R}} f(t) \psi_{u,s}^*(t) dt \tag{3}$$

Here, $*$ denotes the complex conjugate of the function and $\psi_{u,s}(t) = \frac{1}{\sqrt{|s|}} \psi(\frac{t-u}{s})$. The normalization factor $\frac{1}{\sqrt{|s|}}$ ensures that $\|\psi_{u,s}\|_{\mathcal{L}_2}$ remains independent of the translation parameter (u) and the scale ($s > 0$). It has been shown that the information regarding the local singularity(Hölder) exponent can be extracted by following the decay of $|WT_f(u, s)|$ over the finer scales in the

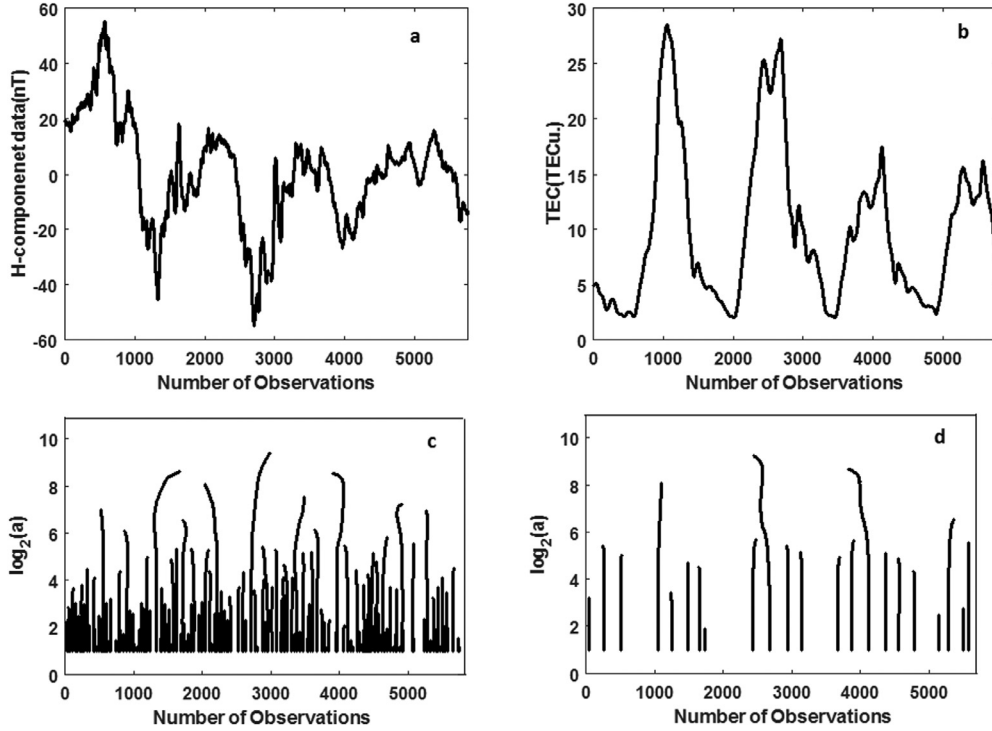


Fig. 2. a) H-component data recorded at SJG and (b) TEC data recorded at CRO1 during the 26-28 March 2008 storm event. Corresponding Lines of maxima of wavelet transform obtained using the first derivative of the Gaussian wavelet c) for the H-component data and d) for TEC data.

neighbourhood of the points, i.e. if the local Hölder exponent of a function f around a point is α , then $|WT_f(u, s)| \leq C|s|^{\alpha+\frac{1}{2}}$ [15,20]. The Gaussian family of wavelets have proven to be very well suited for the purpose of singularity detection because, the use of derivatives of Gaussian as the analyzing wavelet guarantees the propagation of maxima line to the finest scale considered in analysis [11,20]. These wavelets are obtained by taking successive derivatives of Gaussian function. A Gaussian wavelet of order N is defined as $\psi_g^N(t) = \frac{d^N}{dt^N} e^{-\frac{t^2}{2}}$, which will have N vanishing moments and nullifies all the local polynomial trends upto degree $N - 1$. If ψ_g^N has N vanishing moments, then for all m , $0 \leq m < N$, we have $\int_{\mathbb{R}} t^m \psi_g^N(t) dt = 0$. Using these properties one can define a wavelet transform modulus maxima (WTMM) [9–11,19,20,22,36], as the local maxima at each scale s , of the modulus of wavelet transform. WTMM is a process of estimating the multifractal attributes of the data using a set of curves, called lines of maxima (LoM) in the time-frequency plane. These LoM converge to several points on the translation (time) axis as scale $s \rightarrow 0$, signifying the occurrences of singularities in the data at those times. The nature of singularities can be seen from the power law behaviour of the modulus of wavelet transform along the maxima lines as a function of scale [11,19,20]. Fig. 2 depicts the H-component data (Fig. 2a), TEC data (Fig. 2b) and their respective LoM (Fig. 2c and d) corresponding to a geomagnetic storm event of March 2008, recorded at low-latitude region.

As proposed by Arneodo et al. [22,37], Holschneider et al. [38] and Muzy et al. [19], one can define the partition function using the wavelet transform coefficients as:

$$\mathcal{Z}(q, s) = \sum_{l \in \mathcal{L}(a)} \left[\sup_{(\tau, s') \in l, s' < s} |WT_f(\tau, s')| \right]^q \quad (4)$$

Here $\mathcal{L}(a)$ is the set of maxima lines that converges to the singular point in the domain of f . The 'sup' in Eq. (4) implies that for any particular scale of interest, say, s_1 , all the wavelet coefficients that are below s_1 and lie on the LoM are considered and supre-

imum is calculated. Then the coefficient at s_1 will be replaced by the supremum, before proceeding for further analysis [35,38]. Eq. (4) also implies that at $q = 0$, $\mathcal{Z}(0, s) = N_s$, where N_s is the number of maxima lines at the scale, s . The effectiveness of using this partition function is explained in Muzy et al. [12,19] and Venugopal et al. [24]. For different values of $q \in \mathbb{R}$, as $s \rightarrow 0$, $\mathcal{Z}(q, s)$ behaves as

$$\mathcal{Z}(q, s) \sim s^{\tau(q)} \quad (5)$$

By taking the Legendre transform of $\tau(q)$ one can obtain the spectrum of singularities $D(h)$ as [20].

$$D(h) = \min_{q \in \mathbb{R}} [qh - \tau(q)] \quad (6)$$

The behaviour of $\tau(q)$ around $q = 0$ indicates the degree of multifractality of a signal. In particular if $\tau(q)$ is linear or $\frac{d^2\tau(q)}{dq^2} \Big|_{q=0} = 0$, then that indicates the monofractal behaviour of the data. Alternatively, around $q = 0$, if $\frac{d^2\tau(q)}{dq^2} \Big|_{q=0} < 0$, then there exist many scaling exponents resulting in multifractal behavior of the data and thus the large negative values indicate higher degree of multifractality and vice-versa [12,20]. Also for the continuously differentiable $\tau(q)$, the following relationships hold

$$q = \frac{dD(h)}{dh} \quad (7)$$

$$\tau(q) = qh - D(h) \quad (8)$$

and equivalently,

$$h(q) = \frac{d\tau(q)}{dq} \quad (9)$$

This completes the multifractal formalism. In summary, the nature of multifractal attributes like $\tau(q)$, $h(q)$, and $D(h)$ provide information about the scaling behaviour of multifractal process. The computation of $D(h)$ vs. h curve can be understood as the computation of entropy vs. internal energy of a multibody system.

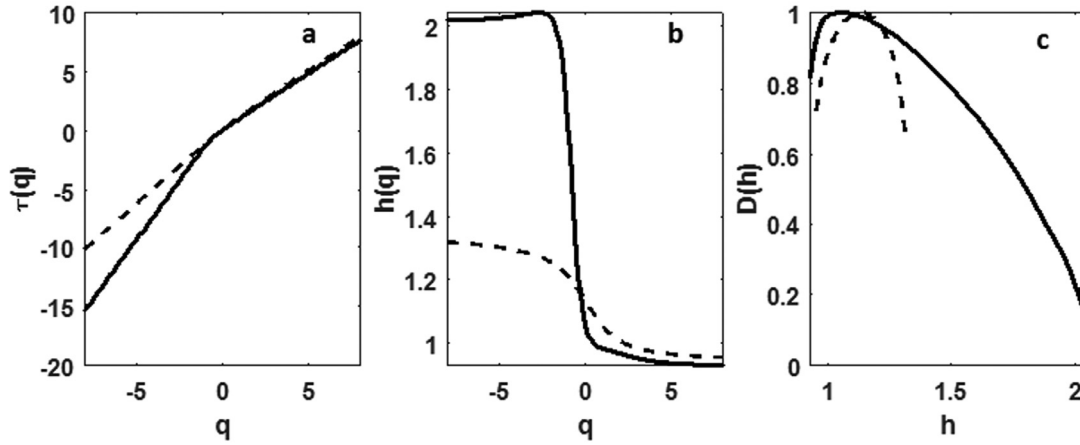


Fig. 3. Multifractal attributes of the data in Fig. 2 obtained using cumulants of wavelet transform. Solid lines (H-component data) and dashed lines (TEC data) represent the variation of (a) the scaling exponent, $\tau(q)$ as a function of order of moments q (b) the generalized Hurst exponent, $h(q)$ as a function of order of moments q and (c) the multifractal singularity spectrum.

The quantities q and $\tau(q)$ have a similar analogous meaning in thermodynamics (Arneodo et al. [22] and references therein). With the help of $\tau(q)$ determined from Eq. (5), one can assess the degree of multifractality by inspecting the non linear behavior of $\tau(q)$ within the small neighborhood of $q = 0$ (Fig. 3a). The extent of nonlinearity observed in the $q - \tau(q)$ curve determines the degree of multifractality in the data. The generalized Hölder exponents $h(q)$ can be derived from $\tau(q)$ (see Eq. 9 and Fig. 3b). Equation (6) is then used to obtain the singularity spectrum. The width of singularity spectrum is proportional to the degree of multifractality of the data (Fig. 3c). However, the multifractal spectra estimated using the above method has been found to be taking longer time for larger data sets. As advocated by [23,24] the efficacy in the computation of multifractal spectra can be improved by using magnitude cumulants of the wavelet transform rather than the wavelet transform coefficients themselves. In the following section, we provide a brief description of the methodology of estimating the multifractal spectra using magnitude cumulants of wavelet transform and its application to the present data.

3.3. Estimation of multifractal attributes using cumulants of wavelet transform

If X is a random variable with pdf $\mathcal{P}(x)$ as probability density function, then we can define a characteristic function or moment generating function $\Phi_x(k)$ (Here $x \in \mathbb{R}$ is the value that the random variable X takes) associated with it as,

$$\Phi_x(k) = \mathbb{E}[e^{ikx}] = \int_{-\infty}^{\infty} e^{ikx} \mathcal{P}(x) dx \tag{10}$$

Here $\mathbb{E}(\cdot)$ is the expectation operator. Also, equivalently,

$$\Phi_x(k) = \mathbb{E}[e^{ikx}] = \mathbb{E}\left[\sum_{n=0}^{\infty} \frac{(ikx)^n}{n!}\right].$$

Using the linearity property of expectation operator, we obtain,

$$\Phi_x(k) = 1 + \sum_{n=1}^{\infty} M_n \frac{(ik)^n}{n!}$$

where,

$$M_n = \int_{-\infty}^{\infty} x^n \mathcal{P}(x) dx$$

is the n^{th} order non-central moment of X for $n = 1, 2, \dots$. Similarly, cumulant generating function of X , $\Psi_x(k)$ is given by

$$\Psi_x(k) = \log \Phi_x(k) \tag{11}$$

$\Psi_x(k)$ has the power series expansion of the form,

$$\Psi_x(k) = \log \mathbb{E}[e^{ikx}] = \sum_{n=1}^{\infty} C_n \frac{(ik)^n}{n!} \tag{12}$$

C_n are the n^{th} order cumulants of X . Value of the C_n can be obtained as,

$$C_n = (i)^{-n} \frac{d^n}{dk^n} \Psi_x(k) \Big|_{k=0} \tag{13}$$

Also,

$$\begin{aligned} \Psi_x(k) &= \log \Phi_x(k) \\ &= \log \left[1 + M_1 \frac{(ik)}{1!} + M_2 \frac{(ik)^2}{2!} + M_3 \frac{(ik)^3}{3!} + \dots \right] \end{aligned}$$

Using

$$\log(1+r) = r - \frac{r^2}{2!} + \frac{r^3}{3!} - \frac{r^4}{4!} + \dots$$

where,

$$r \equiv M_1 \frac{(ik)}{1!} + M_2 \frac{(ik)^2}{2!} + M_3 \frac{(ik)^3}{3!} + \dots$$

So,

$$\begin{aligned} \Psi_x(k) &= M_1 (ik) + (M_2 - M_1^2) \frac{(ik)^2}{2!} + \\ &\quad (M_3 - 3M_1M_2 + M_1^3) \frac{(ik)^3}{3!} + \dots \end{aligned} \tag{14}$$

From Eqs. (13) and (14) its easy to verify that cumulants and moments are related to each other in the following way,

$$\begin{aligned} C_1 &= M_1 \\ C_2 &= M_2 - M_1^2 \\ C_3 &= M_3 - 3M_2M_1 + M_1^3 \\ &\vdots \end{aligned}$$

More details on moments, cumulants and the relation between them can be found in [39]. The behaviour of $|WT_s(\tau, s)|^q$ as a function of scale s (see Eq. (4)), can be written to denote its dependence only on the scales as,

$$\mathbb{E}[|WT_s|^q] = \mathbb{E}[e^{q \log |WT_s|}] \tag{15}$$

Since, we are only interested in calculating the sum of modulus maxima over the lines of maxima, from Equation (4) we have

$$\mathbb{E}[|WT_s|^q] = \frac{1}{N_s} \mathcal{Z}(q, s) \tag{16}$$

Where N_s is the number of maxima lines at a scale s and it has a power law relation with s . $N_s \sim s^{-d_f}$, d_f is the fractal dimension of the support of singularities. Noting that $\mathcal{Z}(q, a) \sim s^{\tau(q)}$ [20], we have

$$\mathbb{E}[|WT_s|^q] \sim \frac{1}{s^{-d_f}} s^{\tau(q)} \sim s^{\tau(q)+d_f} \tag{17}$$

Therefore,

$$s^{\tau(q)+d_f} \sim \mathbb{E}[e^{q \log |WT_s|}] \tag{18}$$

$$\Rightarrow [\tau(q) + d_f] \log s \sim \log \{ \mathbb{E}[e^{q \log |WT_s|}] \} \tag{19}$$

using eq. (12) it can be seen that

$$\log \{ \mathbb{E}[e^{q \log |WT_s|}] \} = \log \{ \mathbb{E}[e^{q i (\log |WT_s|)/i}] \} = \sum_{n=1}^{\infty} \kappa_n \frac{(iq)^n}{n!} \tag{20}$$

Here, κ_n are the cumulants of $\frac{\log |WT_s|}{i}$. So, $C_n = \kappa_n \times (i)^n$ are the cumulants of $\log |WT_s|$ [23][24]. Now rearranging the terms in eq. (20) and substituting it in eq. (19) we, get

$$\sum_{n=1}^{\infty} C_n(s) \frac{q^n}{n!} \sim [\tau(q) + d_f] \log s \tag{21}$$

or

$$-d_f \log s + \sum_{n=1}^{\infty} C_n(s) \frac{q^n}{n!} \sim \tau(q) \log s \tag{22}$$

Where,

$$C_1(s) \equiv \mathbb{E}[\log |WT_s|] \sim c_1 \log(s) \tag{23}$$

$$C_2(s) \equiv \mathbb{E}[\log^2 |WT_s|] - [\mathbb{E}[\log |WT_s|]]^2 \sim -c_2 \log(s) \tag{24}$$

$$C_3(s) \equiv \mathbb{E}[\log^3 |WT_s|] - 3\mathbb{E}[\log^2 |WT_s|]\mathbb{E}[\log |WT_s|] + [\mathbb{E}[\log |WT_s|]]^3 \sim c_3 \log(s) \tag{25}$$

⋮

so, it can now be easily seen that

$$\begin{aligned} \tau(q) &= -d_f \frac{q^0}{0!} + \sum_{n=1}^{\infty} \left[\frac{C_n(s)}{\log s} \right] \frac{q^n}{n!} \\ &= -c_0 + c_1 \frac{q}{1!} - c_2 \frac{q^2}{2!} + c_3 \frac{q^3}{3!} - \dots \end{aligned} \tag{26}$$

From the above it can easily be seen that one can estimate $\tau(q)$ and the $D(h)$ curves using the polynomial expansion of Eqs. (26) and (6). For most of the practical purposes, a quadratic approximation of $\tau(q)$ will be sufficient for correctly estimating the multifractal behaviour of the signal under consideration. For the multifractal processes that have quadratic $\tau(q)$ and $D(h)$, the following relation holds [23,24]

$$D(h) = c_0 - \frac{(h - c_1)^2}{2c_2} \tag{27}$$

This presents a major advantage over the other wavelet based methods like WTMM, where for estimating $\tau(q)$ one has to analyze the behaviour of $\mathcal{Z}(q, s)$ for a large number of q values. From Eq. (26) it can be seen that for a monofractal signal (linear $\tau(q)$) only two regressions are needed (c_0 and c_1) and in the case of multifractals one has to perform three regressions (c_0, c_1, c_2) to obtain a quadratic approximation of $\tau(q)$. This reduces the computational time to a great extent even for very large data sets. Fig. 4 shows the comparison of singularity spectrum obtained for TEC and H-component data using WTMM and magnitude cumulant of wavelet transform. The spectrum obtained using WTMM is similar to the one obtained using magnitude cumulants of wavelet transforms. Similar results were obtained for other sites also. However, because of its computational efficiency, the magnitude cumulant of wavelet transform is used in further analysis.

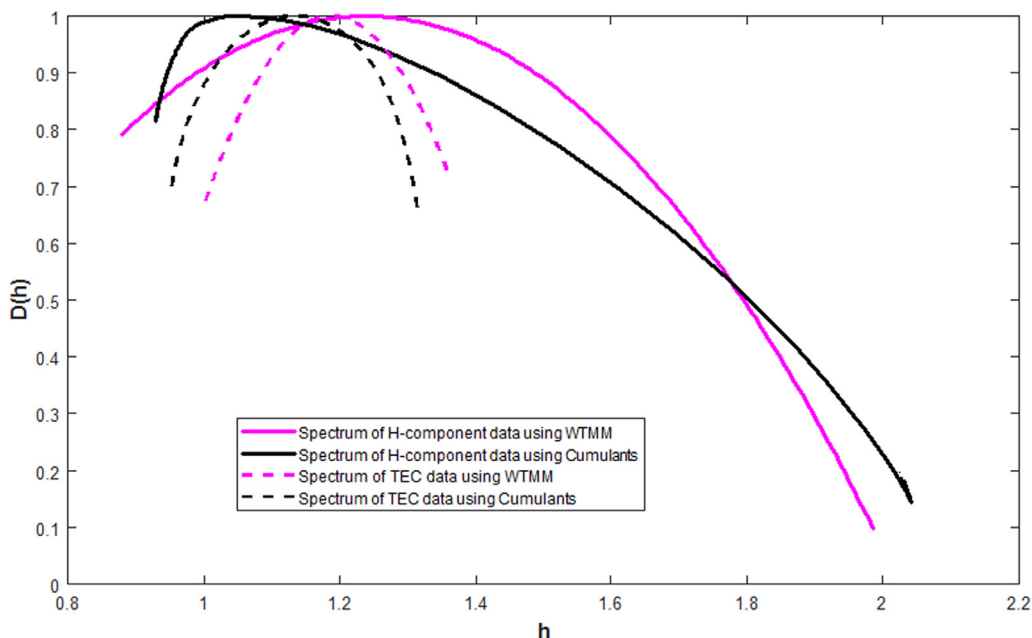


Fig. 4. Comparison of the singularity spectra obtained for H-component and TEC data corresponding to CRO1 and SJG sites (lower latitude region) using WTMM and cumulant based multifractal analysis corresponding to March, 2008.

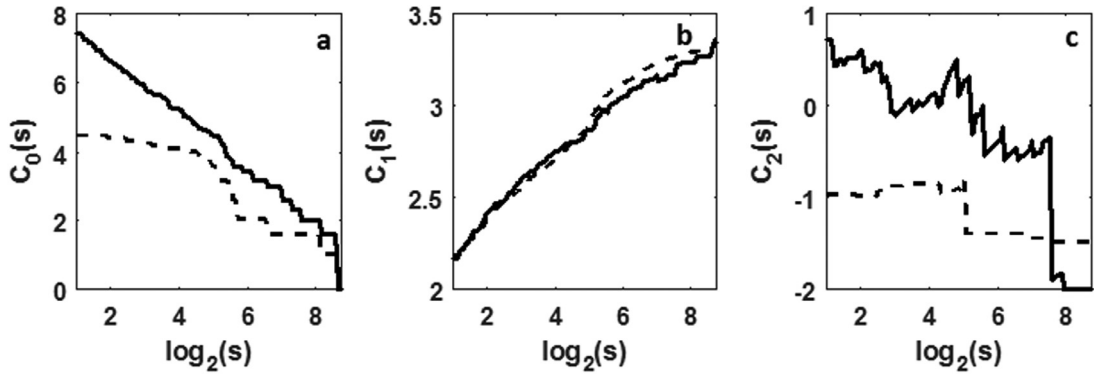


Fig. 5. $C_n(s)$ (Eq. 26) corresponding to the H-component (solid curves) and TEC (dashed curves) data shown in Fig. 2. For (a) $n = 0$ (b) $n = 1$ (c) $n = 2$.

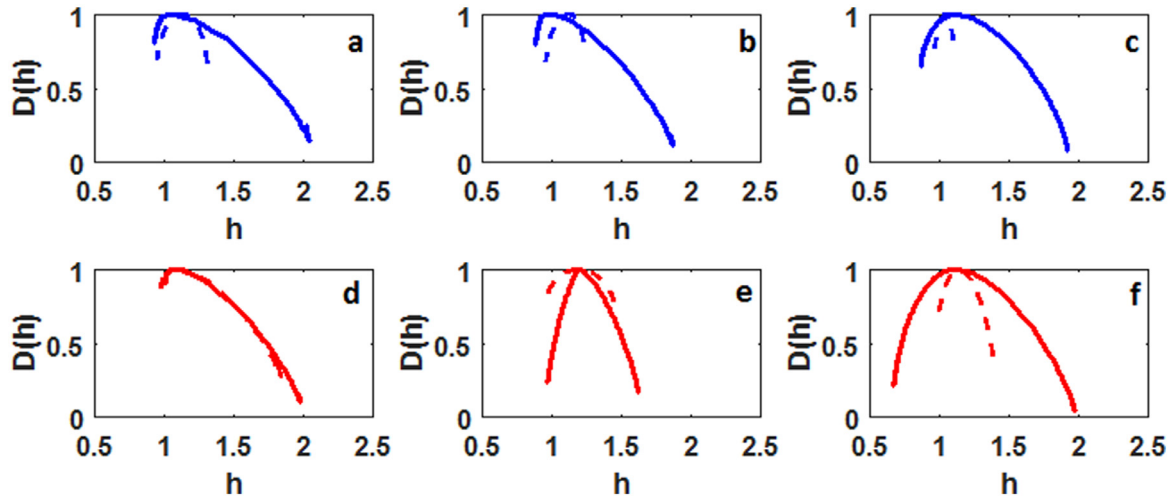


Fig. 6. Multifractal singularity spectra of the H-component data (solid curves) and TEC data (dashed curves) of low latitude stations (a,d), mid-latitude stations (b,e) and high-latitude stations (c,f) corresponding to the storm event occurred in the month of March during the solar minimum year (2008) (blue curves) and the solar maximum year (2014) (red curves). See Tables 1 and 2.

The multifractality of H-component data and TEC can also be inferred from the variation of cumulants of wavelet transform (see Eq. 21) as the function of scales. Using Eqs. (21) and (26), one can obtain the cumulants (C 's) and then the coefficients (c 's) of the polynomial approximation of $\tau(q)$. Also, from Eqs (21) and (26), it can be seen that the coefficients (c 's) designate the slopes of the plots drawn between cumulants (C 's) and the logarithm of scales. Fig. 5 shows the variation of the cumulants $C_n(s)$ as the function of scale s for $n = 0, 1, 2$.

Figs. 6 and 7 show the examples of multifractal singularity spectra determined for H-component and TEC data for different latitude zones (see Table 1) during storm events in the months of March and August respectively (see Table 2).

3.4. Multifractal cascades and the P-model

Due to scale dependent nature of multifractal processes, additive linear models like ARIMA tend to be insufficient for a complete description (or modelling) of the underlined multifractal phenomena. Therefore, to understand the relation between different multifractal singularity spectra (see Figs. 3c, 6 and 7) and their respective multiplicative cascade system, a non-linear P-model was fit to the multifractal spectra obtained for various storm events (see Table 2) [28,29]. This model brings out the information about the degree of multifractality of the data using a parameter P that can be used to quantify the spectral width of the process. According to the P-model, the singularity exponents h

and their Hausdorff dimensions $D(h)$ are related to each other via the non-linear relation (see, [28,29])

$$h = - \frac{w \log P + (1 - w) \log(1 - P)}{\log 2} \tag{28}$$

$$D(h) = - \frac{w \log w + (1 - w) \log(1 - w)}{\log 2} \tag{29}$$

This model involves the partitioning of a unit line segment into two equal sub-segments. The concentration value (ρ) of the quantity (TEC or H-component data) in the unit segment can be written as ρP for one half and $\rho(1 - P)$ for the other half ($0 < P < 1$), such that the total mass is conserved. At the beginning of the process ρ can be set equal to 1. The dispersion coefficient (P) is independent of the length of the segment. If the value of $P > 0.5$, then the maximum and minimum element concentration after n subdivision are respectively P^n and $(1 - P)^n$. However, for $P < 0.5$, the maximum and minimum element concentrations are reversed and thus they become $(1 - P)^n$ and P^n respectively. For a particular segment after n subdivision the general concentration is $P^k(1 - P)^{n-k}$ ($0 \leq k \leq n$). From these, one can eliminate the variable $w = \frac{k}{n}$ and obtain the expression for $D(h)$ in terms of h and parameters P and thus nonlinear leastsquares can be applied to obtain the value of these parameters corresponding to the multifractal spectrum [28,29,40]. Results of P-model fitting to the multifractal spectra corresponding to different latitude zones are discussed in the next section.

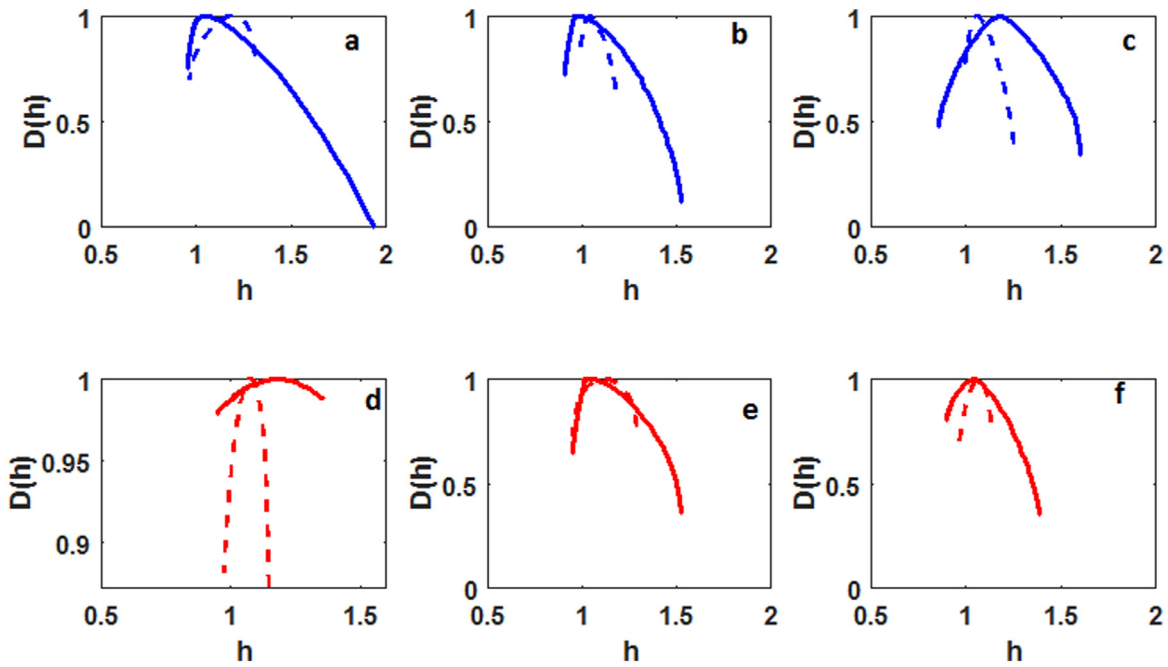


Fig. 7. Same as Fig. 6, but for the month of August.

4. Results and Discussion

4.1. Multifractal analysis of TEC and H-Component data

Various methods of multifractal analysis provide similar information regarding different multifractal attributes of the same data. Analysis based on the cumulants of CWT coefficients is advantageous because, the number of regressions needed to estimate different multifractal attributes is greatly reduced (see Section 3.3).

Fig. 3 shows various multifractal attributes corresponding to the H-component and TEC data shown in Fig. 2. The linear behaviour of $\tau(q)$ for all q (Fig. 3a) suggests a monofractal behaviour of TEC. However, the behaviour of $\tau(q)$ observed around $q=0$ for H-component data (Fig. 3a) is nonlinear. This suggests that the $\tau(q)$ estimated for H-component data (Eq. 26) involves more coefficients (higher order q terms) in its polynomial expansion, making its behaviour nonlinear with respect to q . According to Eq (9), this results in estimation of more number of Hölder exponents to characterize the nonlinear behaviour of H-component data. Fig. 3b shows that the variation of $h(q)$ with respect to q is large (small) for H-component (TEC) data. This further justifies the monofractal behaviour of the TEC data, while H-component data displays multifractal behaviour. This is expected because, the TEC data generally exhibits a quasi-periodic nature (Fig. 2b) compared to H-component data (Fig. 2a) and thus they are less stochastic than H-component data, regardless of solar conditions. The widths of the singularity spectra characterize the degree of multifractality in the data (Kantelhardt et al. [14] and Chandrasekhar et al. [18]). The smaller (broader) width signifies the monofractal (multifractal) behaviour of the data. Accordingly, Fig. 3c displays that the degree of multifractality is high for H-component data compared to TEC data. Hence, all the attributes indicate that the H-component data is more multifractal in nature than the TEC data. This explains that the magnetospheric disturbances during solar active times have larger influences on geomagnetic data than on TEC data, thereby making the former highly chaotic than the latter, even though both are recorded during the same time. Chandrasekhar et al. [18] show that the TEC at all other periods

except at 1-day period shows a higher degree of multifractality during solar maximum compared to solar minimum. The TEC shows a clear monofractal behaviour at 1-day periodicity. The multifractal behaviour of TEC and H-component data determined in the present study with the novel wavelet-based techniques also corroborates these observations (Figs. 6 and 7). Although the TEC and H-component data sets correspond to the same geomagnetic storm event, the multifractal spectral widths are smaller during low solar activity (see Figures (6a,7a), (6b,7b), (6c, 7c)) compared to those during high solar activity (see Figures (6d,7d), (6e,7e), (6f, 7f)). Also from the figures (6b, 7b) & (6e, 7e), we can see that the spectral width of the H-component at mid-latitude stations is less than that of low and high latitude stations. It is well known that the horizontal component of the Earth's magnetic field is abnormal during the geomagnetically disturbed times due to the strong presence of the ring current [41,42] in the equatorial plane. Also stations at higher latitudes are more geomagnetically disturbed than those at low latitudes. However, at mid latitudes, the field aligned currents have the largest contribution to both the H and D magnetic components. The studies of Pulkkinen et al. [43] have shown that the induced geo-electric field magnitudes are smaller by an order at around 50° geomagnetic latitude. Hence the geomagnetic disturbance in the horizontal component are less at mid latitudes compared to those at the equatorial, low latitudes and at high latitudes. This is well reflected in the spectral widths of the horizontal component (Figs. 6 and 7).

Fig. 5 shows the variation of the cumulants $C_n(s)$ as the function of scale s for $n=0, 1, 2$. As explained in the previous section, the coefficients of polynomial expansion c_n (see Eqs. 26 and 27) can be obtained as the slope of straight line fit to the $C_n(s)$ vs $\log s$ curve. From Eq. (26), it can be seen that $c_0 = d_f$, where d_f is the fractal dimension of the support of singularity and is related to the number of maxima lines at a given scale [23]. So, a higher value of c_0 indicates the presence of more singularities in the data at lower scales. Accordingly, the H-component data that shows higher c_0 value compared to TEC data (Fig. 5a) has more singularities in it (Fig. 2c) than TEC (Fig. 2d). The value of c_1 represents the mean h (the value of h for which $D(h)$ is maximum i.e., $D(h) = 1$ in our

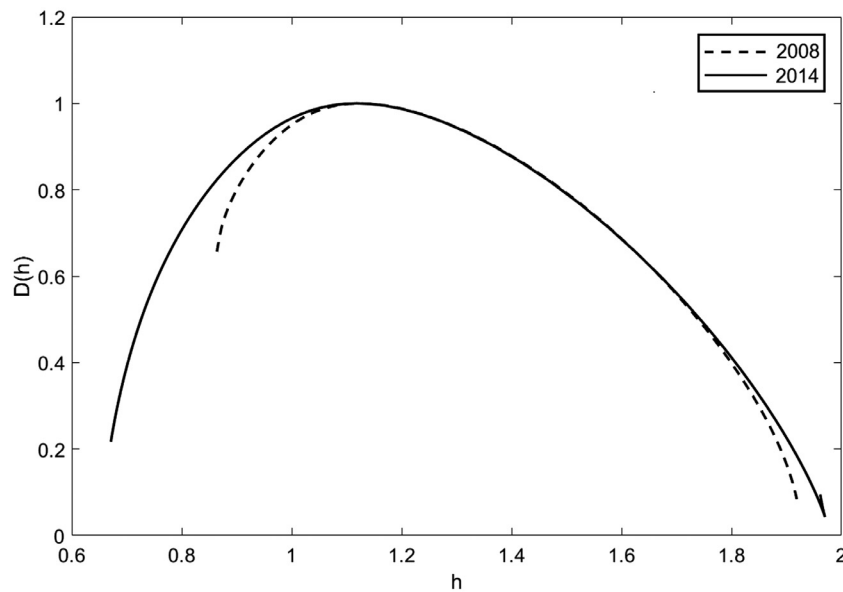


Fig. 8. Multifractal singularity spectra of H-component data corresponding to NAQ (see Table 1) for a storm event in the month of August (see Table 2).

case) as the scale $s \rightarrow 0$ [23]. It can be clearly seen from Fig. 5b that both for the H-component data and TEC data, the straight line fit to the $C_1(s)$ vs. $\log s$ curve results in an identical slope, resulting in the mean h value for both the data sets to be identical. This can be clearly seen in Fig. 3c, where the multifractal spectra of TEC and H-component coincide at $D(h) = 1$. The coefficient c_2 is related to the 2nd order derivative of $\tau(q)$ in the neighborhood of $q = 0$. The magnitude of c_2 indicates the degree of nonlinearity of $\tau(q)$ in the neighborhood of $q = 0$. Hence, it can be seen from Fig. 5c that the magnitude of the slope of a straight line fit for $C_2(s)$ vs. $\log s$ curve for H-component (TEC) data is large (small), resulting in the larger (smaller) multifractal spectral width (Fig. 3c). The nature of c_0 , c_1

and c_2 coefficients have been observed to be similar for all the storm events corresponding to solar minimum (2008) and maximum (2014) years shown in Table 2. The smaller multifractal spectral widths for TEC data (Figs. 3c, 6 and 7) signify their monofractal behaviour, which can be attributed to their quasi-periodic nature with a fundamental period of about 1 day [18]. The widths of multifractal singularity spectra of H-component data (Figs. 3c, 6 and 7) are larger compared to those of TEC, signifying their multifractal behaviour, which can be attributed to their highly stochastic and chaotic nature during different solar conditions. Even among the H-component data alone, the spectral width for 2014 data are higher compared to 2008 data recorded at the same site (Fig. 8).

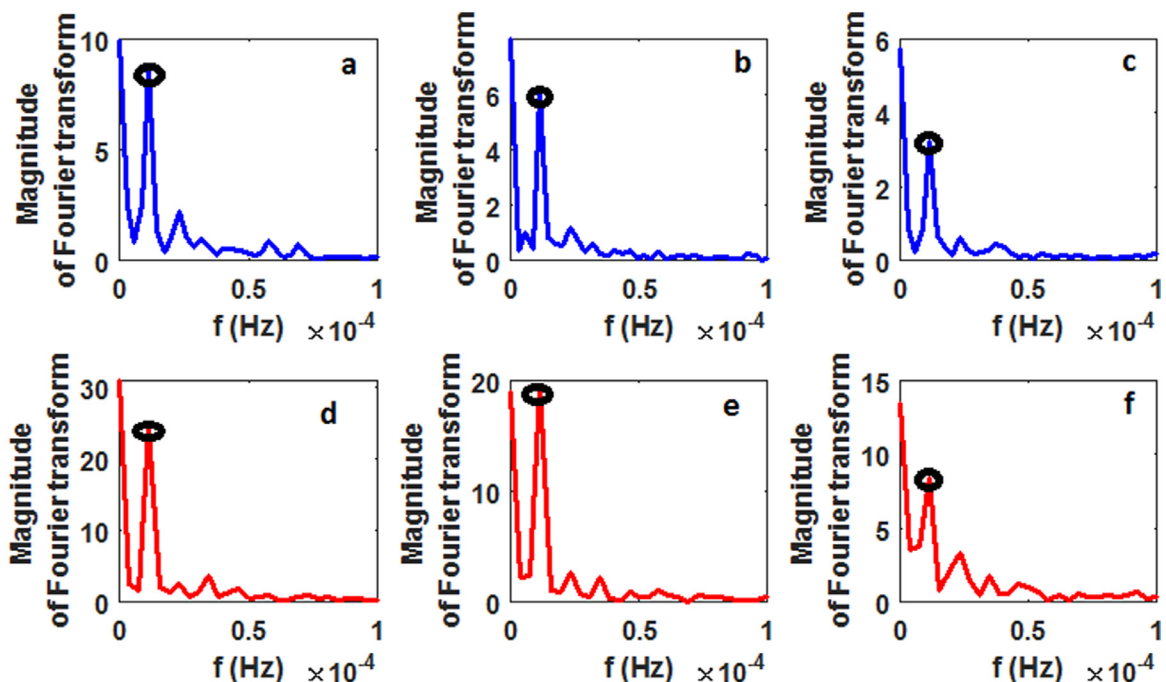


Fig. 9. Fourier transform of raw TEC data during a geomagnetic storm event in March during solar minimum year (2008) (blue curves) and solar maximum year (2014) (red curves) for low-latitudes (a,d), mid-latitudes (b,e) and high-latitudes (c,f). Dominant diurnal component is indicated with black circles.

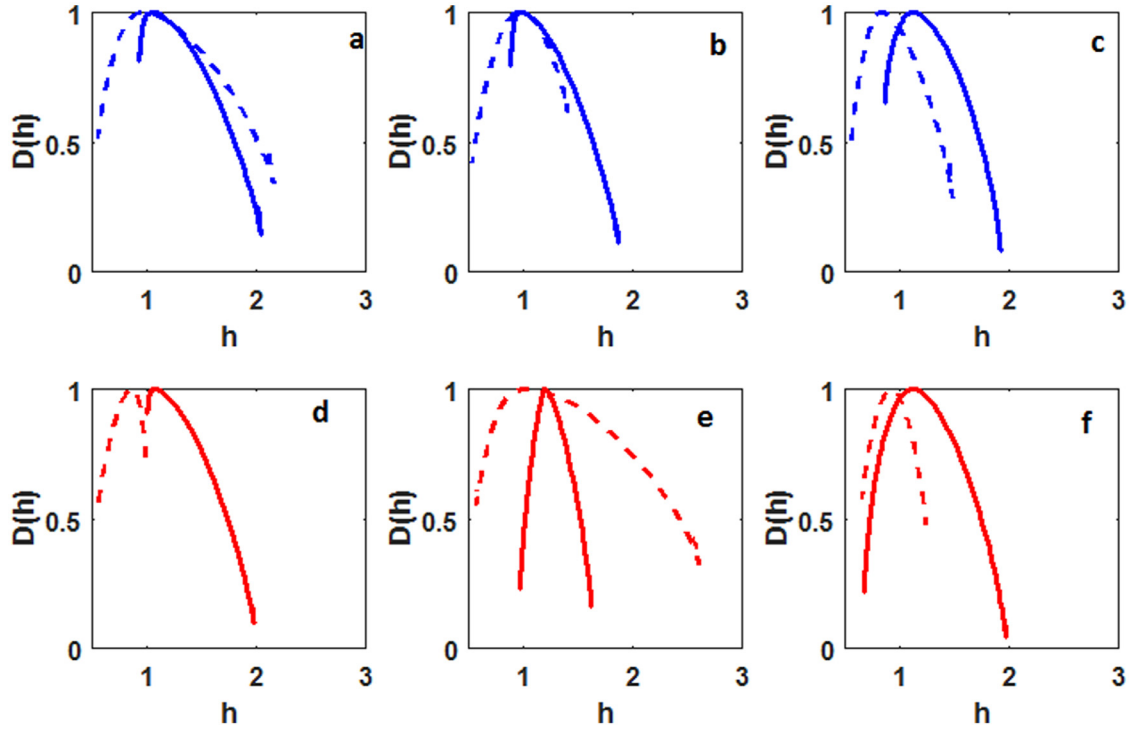


Fig. 10. Multifractal singularity spectra of the H-component data (solid line) and filtered TEC data with diurnal component removed (dashed line) for low latitude stations (a,d), mid-latitude stations (b,e) and high-latitude stations (c,f) corresponding to the storm event occurred in the month of March during the solar minimum year (2008) (blue curves) and the solar maximum year (2014) (red curves). See Tables 1 and 2.

This further confirms that the higher degree of stochasticity in the data results in larger multifractal spectral width and vice-versa. The singularity spectrum corresponding to the H-component data is always right skewed. In general, while a right-skewed multifractal spectrum signifies strongly weighted high fractal exponents, corresponding to finer structures present in the data, the relatively low values of fractal exponents, representative of the presence of coarser structures account for left-skewed spectra [14,18].

Fig. 9 shows the Fourier transform of TEC data for low-latitude stations (9a, 9d), mid-latitude stations (9b, 9e) and high-latitude stations (9c, 9f) corresponding to a storm event in month of March during solar minimum year (2008) (blue) curves and solar maximum year (2014) (red curves). It is evident in all these cases that, sinusoids having one day period are dominant in the data. These dominant sinusoids are the main reason for diurnal behavior of TEC data. So, there is a possibility that many singularities are hidden or remain undetected in the usual multifractal analysis. To detect those singularities, we first filter the raw TEC data using a highpass zero-phase distortion IIR filter. The passband frequency for this filter is chosen to be 1.33×10^{-5} Hz, corresponding to the sinusoid having a fundamental period of 20 hours. It can be observed from Figs. 10a--f and 11 a--f that the widths of the multifractal spectra of the TEC data significantly increase after the diurnal frequency is filtered out from the data, compared to those shown in Figs. 6a--f and 7a--f, which have the diurnal frequencies present in the data. This shows that the singularities in the TEC data are masked by the presence of dominant diurnal component. Also, the mean singularity (value of h for which $D(h) = 1$) in the case of filtered TEC data is always less than that of the H-component data. This can be attributed to the presence of a fewer number of cycles present in the filtered TEC data, compared to those in the H-component data [18].

Fig. 12 shows the singularity spectra and their P-model model fit for different latitude locations corresponding to a storm event in March 2008. Cheng [29] showed that the value of the parameter

P is directly proportional to the spectral width (Δh) of the process as

$$\Delta h \propto \log \frac{P}{1-P} \quad (30)$$

where the proportionality constant is equal to $\frac{1}{\log 2}$. Fig. 12 shows quite a good fit between the estimated P-models and their respective multifractal spectra for H-component and TEC data of a geomagnetic storm event of 2008, corresponding to lower (Fig. 12a, d), middle (Fig. 12b, e) and higher (Fig. 12c, f) latitude zones. It is noteworthy that the P-model estimates for H-component data are higher than that for TEC data. It is also interesting to note the increase in P-model values for the TEC data, when the diurnal frequency component is filtered out from it (Figs. 11d--f). Similar behaviour was observed for both the data sets of 2014. This further confirms the persistent higher degree of stochasticity present in H-component data than in TEC data, regardless of solar conditions. Since we have considered symmetric multiplicative cascades in estimating the P-model (see Section 3.4), the multifractal spectrum that is more symmetric will fit well with the P-model. Accordingly, as can be seen in Fig. 12, the P-model fitting for TEC data is better, compared to that for H-component data.

4.2. Statistical Hypothesis Testing

For testing the statistical significance of the results, bootstrapping technique as described in [44] is used. For a given time-series several instances of shuffled data (1000 in the present study) are generated to remove any temporal correlation that exist in the data. Multifractal analysis is then carried out using the same method as described above. Since an uncorrelated time-series exhibits a monofractal behavior (linear $\tau(q)$) [22,37], it should result a smaller spectral width. Therefore, if we denote the shuffled time series for TEC and H-component data as tec_{md} and mag_{md} , then the width of multifractal spectrum of the shuffled time series

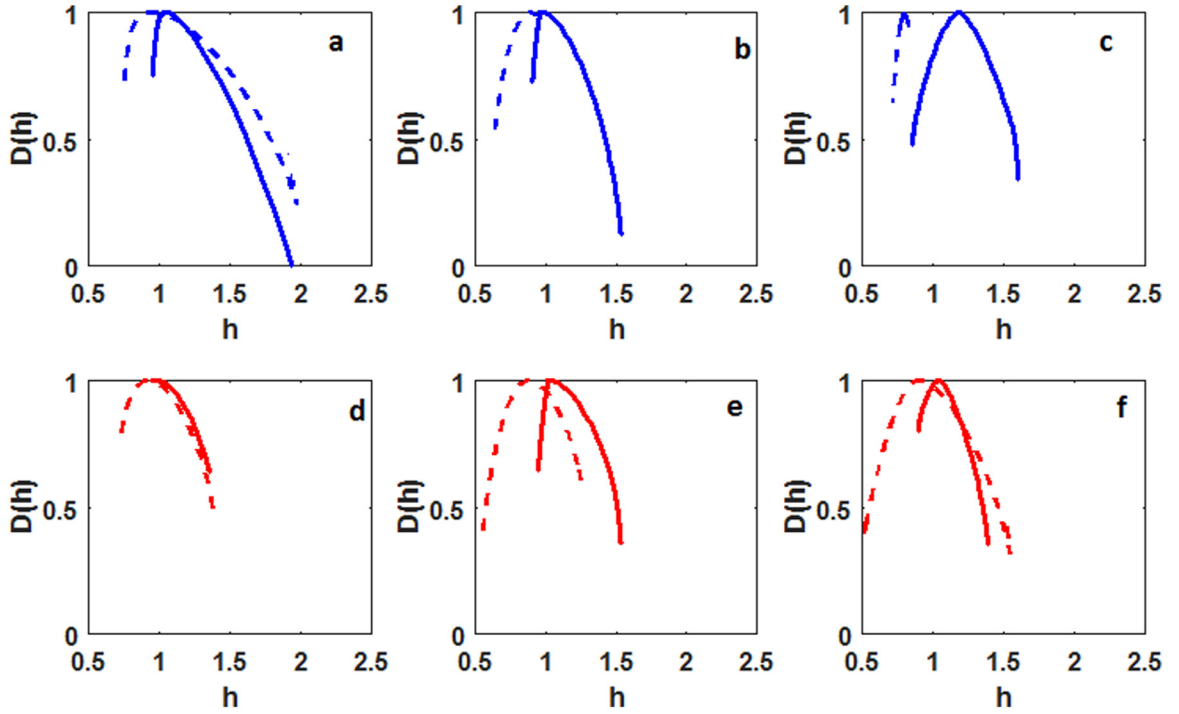


Fig. 11. Same as Fig. 10, but for the month of August.

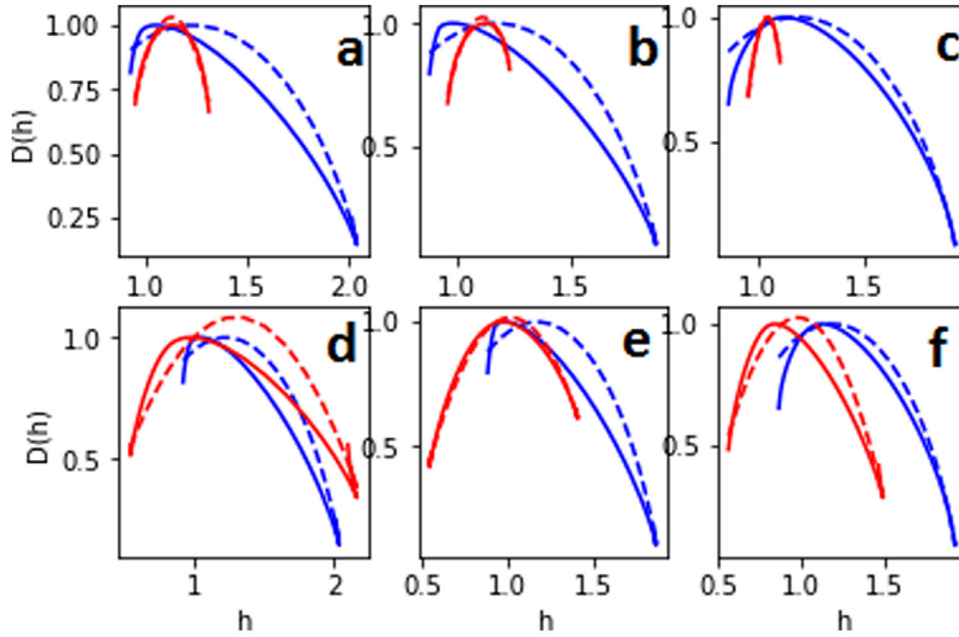


Fig. 12. P-model fit (dashed-lines) for the multifractal spectra (solid-lines) of H-component data (blue curves) and TEC data (red curves) for lower latitudes (a,d), middle latitudes (b,e) and higher latitudes (c,f) for a geomagnetic storm event of March 2008. Red curves in d,e,f represent the multifractal spectra and P-model fits for the TEC data after removing the diurnal component. $P_{tec}(P_{mag})$ is the value of the parameter P for the TEC (H-component) data. For (a) lower lat. $P_{tec} = 0.055$ ($P_{mag} = 0.2368$) (b) middle lat. $P_{tec} = 0.088$ ($P_{mag} = 0.273$) (c) higher lat. $P_{tec} = 0.140$ ($P_{mag} = 0.307$). Similarly, after removing the diurnal component, (d) $P_{tec} = 0.277$, (e) $P_{tec} = 0.2698$, (f) $P_{tec} = 0.2616$.

$\Delta h_{tec_{rnd}}$ (or $\Delta h_{mag_{rnd}}$) will be less than that of original data Δh_{tec} (or Δh_{mag}). Therefore, to test this, we establish a null hypothesis

$$H_0 : \Delta h_{tec_{rnd}} (\Delta h_{Mag_{rnd}}) \geq \Delta h_{tec} (\Delta h_{Mag}) \quad (31)$$

For statistical significance of the empirical results, this hypothesis should be rejected for every shuffled sequence. So, the probability of H_0 , expressed as $p = P(H_0)$, is calculated. Under the conventional significance level of 0.05, the multifractal phenomenon

is statistically significant if and only if $p \leq 0.05$. Table 3 gives the estimated probability values for TEC data and H-component data of all the sites (Table 1). It can be seen from Table 3 the very low probability values suggest that the the null hypothesis, H_0 (Eq. 29), is rejected and thus the width of multifractal spectrum of the shuffled time series $\Delta h_{tec_{rnd}}$ (or $\Delta h_{mag_{rnd}}$) has always been less than that of original data Δh_{tec} (or Δh_{mag}). This shows that the results are statistically significant having a significance level of 95%.

Table 3

Estimated p -values ($p=P(H_0)$) (see Section 4.2) for magnetic observatory sites (1-3) and TEC sites (4-6) for different storms of the years 2008 and 2014 (see Table 2).

S.No.	Site Code	Feb 2008 (2014)	March 2008 (2014)	Aug. 2008 (2014)	Sept. 2008 (2014)	Oct. 2008 (2014)
1	SJG	0(0)	0(0)	0(0.005)	0.002(0.001)	0(0)
2	OTT	0(0.002)	0.001(0)	0(0)	0(0)	0(0.001)
3	NAQ	0.01(0)	0(0.003)	0.001(0)	0(0)	0.001(0.002)
4	CRO1	0.002(0.001)	0(0)	0.004(0.004)	0(0.001)	0.001(0.002)
5	ALGO	0(0)	0.003(0)	0.001(0.003)	0.002(0.001)	0(0)
6	QAQ1	0(0.001)	0.0(0.003)	0(0.002)	0(0)	0(0.003)

5. Conclusions

The multifractal behaviour of the ionospheric TEC data vis-a-vis the H-component data during different solar conditions has been studied using the cumulants of magnitudes of wavelet transform coefficients. The advantage of determining the multifractal behaviour of nonlinear data using cumulants over the WTMM method is, in WTMM method, for estimating the multifractal attribute, $\tau(q)$, one has to analyze the behaviour of the partition function $Z(q, s)$ for a large range of q values. Whereas, with cumulants of wavelet transform coefficients, $\tau(q)$ can be easily estimated by making the polynomial expansion of $\tau(q)$ (see Eq. 26) up to three terms only. The results clearly explain that the degree of stochasticity in H-component data is relatively higher than that in TEC data at all latitude zones, regardless of solar conditions. These observations have also been validated by fitting a nonlinear P-model, representative of multiplicative cascades to the multifractal singularity spectrum. It was also noticed that the spectral width for the H-component data was less at mid-latitudes compared to that of low and high latitudes. This is because, the induced geo-electric field magnitudes are smaller by an order at around 50° geomagnetic latitude. Hence the geomagnetic disturbances in the horizontal component are less at mid latitudes compared to those at the equatorial, low latitudes and at high latitudes. A bootstrapping-based statistical hypothesis testing also establishes the statistical significance of the multifractal behaviour of both the data sets. The lower degree of multifractality observed in TEC data is due to the presence of a strong diurnal component, which masks the singularities in it. This is verified by performing the multifractal analysis of TEC data with and without the dominant diurnal frequency component present in it. The increased multifractal spectral width of the filtered TEC is also reflected by the increased value of P-model estimates (see Fig. 12)

These results further strongly motivate the apt use of application of wavelet transform-based cumulant analysis on various other nonlinear geophysical data sets for their improved understanding and characterization.

Data availability

Data used in the present study are freely downloadable from the following repositories (see also Section 2).

- <http://sopac.ucsd.edu/dataBrowser.shtml>.
- <http://wdc.kugi.kyoto-u.ac.jp/index.html>.
- <http://www.wdc.bgs.ac.uk/data.html>.

Declaration of Competing Interest

The authors declare that they have no known competing financial interests or personal relationships that could have appeared to influence the work reported in this paper.

Acknowledgements

The authors thank SOPAC facility and WDCs for maintaining and making available the high quality TEC data and geomagnetic data respectively, without which the present analysis could not have been possible. One of the authors, SB thanks IIT Bombay for awarding him the necessary fellowship for his Ph.D work.

References

- [1] Pröls G. Physics of the Earth's space environment: an introduction. Springer Science & Business Media; 2012.
- [2] Buonsanto MJ. Ionospheric storms - a review. Space Sci Rev 1999;88(3-4):563-601.
- [3] Gonzalez W, Joselyn J-A, Kamide Y, Kroehl HW, Rostoker G, Tsurutani B. What is a geomagnetic storm? J Geophys Res: Space Phys 1994;99(A4):5771-92.
- [4] Akasofu S-I. Relationships between the ae and dst indices during geomagnetic storms. J Geophys Res: Space Phys 1981;86(A6):4820-2.
- [5] Chapman S. Earth storms: Retrospect and prospect. J Phys Soc Jpn Suppl 1962;17:6.
- [6] Campbell WH. Occurrence of ae and dst geomagnetic index levels and the selection of the quietest days in a year. J Geophys Res: Space Phys 1979;84(A3):875-81.
- [7] Frisch U. Fully developed turbulence and intermittency. Ann New York Acad Sci 1980;357(1):359-67.
- [8] Mandelbrot B., Fisher A., Calvet L. A multifractal model of asset returns 1997.
- [9] Davis A, Marshak A, Wiscombe W, Cahalan R. Multifractal characterizations of nonstationarity and intermittency in geophysical fields: Observed, retrieved, or simulated. J Geophys Res: Atmos 1994;99(D4):8055-72.
- [10] Riedi RH, Crouse MS, Ribeiro VJ, Baraniuk RG. A multifractal wavelet model with application to network traffic. IEEE Trans Inf Theory 1999;45(3):992-1018.
- [11] Mallat S, Hwang WL. Singularity detection and processing with wavelets. IEEE Trans Inf Theory 1992;38(2):617-43.
- [12] Muzy J-F, Bacry E, Arneodo A. Multifractal formalism for fractal signals: The structure-function approach versus the wavelet-transform modulus-maxima method. Phys Rev E 1993;47(2):875.
- [13] Kantelhardt JW, Koscielny-Bunde E, Rego HH, Havlin S, Bunde A. Detecting long-range correlations with detrended fluctuation analysis. Physica A 2001;295(3-4):441-54.
- [14] Kantelhardt JW, Zschiegner SA, Koscielny-Bunde E, Havlin S, Bunde A, Stanley HE. Multifractal detrended fluctuation analysis of nonstationary time series. Physica A 2002;316(1-4):87-114.
- [15] Foufoula-Georgiou E, Kumar P. Wavelets in geophysics, 4. Elsevier; 2014.
- [16] Subhakar D, Chandrasekhar E. Detrended fluctuation analysis of geophysical well-log data. In: Dimri V, editor. Fractal Solutions for Understanding Complex Systems in Earth Sciences. Switzerland: Springer International Publishing; 2015. p. 47-65.
- [17] Subhakar D, Chandrasekhar E. Reservoir characterization using multifractal detrended fluctuation analysis of geophysical well-log data. Physica A 2016;445:57-65.
- [18] Chandrasekhar E, Prabhudesai SS, Seemala GK, Shenoi N. Multifractal detrended fluctuation analysis of ionospheric total electron content data during solar minimum and maximum. J Atmos Solar-Terrestrial Phys 2016;149:31-9.
- [19] Muzy J-F, Bacry E, Arneodo A. The multifractal formalism revisited with wavelets. Int J Bifurc Chaos 1994;4(2):245-302.
- [20] Mallat S. A wavelet tour of signal processing. Elsevier; 1999.
- [21] Daubechies I. Ten lectures on wavelets, 61. Siam; 1992.
- [22] Arneodo A, Bacry E, Muzy J. The thermodynamics of fractals revisited with wavelets. WaveletsPhys 1999;339-90.
- [23] Delour J, Muzy J, Arneodo A. Intermittency of 1d velocity spatial profiles in turbulence: a magnitude cumulant analysis. Eur Phys J B 2001;23(2):243-8.
- [24] Venugopal V, Roux SG, Foufoula-Georgiou E, Arneodo A. Revisiting multifractality of high-resolution temporal rainfall using a wavelet-based formalism. Water Resour Res 2006;42(6).
- [25] Jaffard S. Multifractal formalism for functions part i: results valid for all functions. SIAM J Math Anal 1997;28(4):944-70.
- [26] Jaffard S. Multifractal formalism for functions part ii: self-similar functions. SIAM J Math Anal 1997;28(4):971-98.

- [27] Wendt H, Roux SG, Jaffard S, Abry P. Wavelet leaders and bootstrap for multifractal analysis of images. *Signal Process* 2009;89(6):1100–14.
- [28] Halsey TC, Jensen MH, Kadanoff LP, Procaccia I, Shraiman BI. Fractal measures and their singularities: the characterization of strange sets. *Phys Rev A* 1986;33(2):1141.
- [29] Cheng Q. Generalized binomial multiplicative cascade processes and asymmetrical multifractal distributions. *Nonlinear Process Geophys* 2014;21(2):477–87.
- [30] Meneveau C, Sreenivasan K. Simple multifractal cascade model for fully developed turbulence. *Phys Rev Lett* 1987;59(13):1424.
- [31] Taqqu MS, Teverovsky V, Willinger W. Estimators for long-range dependence: an empirical study. *Fractals* 1995;3(04):785–98.
- [32] Veitch D, Abry P. A wavelet-based joint estimator of the parameters of long-range dependence. *IEEE Trans Inf Theory* 1999;45(3):878–97.
- [33] Sharma M, Vanmali AV, Gadre VM. Construction of wavelets: Principles and practices. In: Chandrasekhar E, Dimri VP, Gadre VM, editors. *Wavelets and Fractals in Earth System Sciences*. CRC Press: Taylor & Francis; 2013. p. 29–92.
- [34] Chandrasekhar E, Rao VE. Wavelet analysis of geophysical well-log data of Bombay offshore basin, India. *Math Geosci* 2012;44(8):901–28.
- [35] Chandrasekhar E, Prasad P, Gurijala V. Geomagnetic jerks: A study using complex wavelets. In: Chandrasekhar E, Dimri VP, Gadre VM, editors. *Wavelets and Fractals in Earth System Sciences*. CRC Press: Taylor & Francis; 2013. p. 195–218.
- [36] Tu C-L, Hwang W-L, Ho J. Analysis of singularities from modulus maxima of complex wavelets. *IEEE Trans Inf Theory* 2005;51(3):1049–62.
- [37] Arneodo A, Grasseau G, Holschneider M. Wavelet transform of multifractals. *Phys Rev Lett* 1988;61(20):2281.
- [38] Holschneider M, Kronland-Martinot R, Morlet J, Tchamitchian P. A real-time algorithm for signal analysis with the help of the wavelet transform. In: *Wavelets*. Springer; 1990. p. 286–97.
- [39] Populis A, Pillai S. *Probability, random variables and stochastic processes*. 4th ed. New York: McGraw Hill; 2002.
- [40] Hosseinabadi S, Rajabpour MA, Movahed MS, Allaei SV. Geometrical exponents of contour loops on synthetic multifractal rough surfaces: Multiplicative hierarchical cascade p model. *Phys Rev E* 2012;85(3):3113.
- [41] Chapman S, Ferraro V. The geomagnetic ring-current: I-its radial stability. *Terrestrial Magnet Atmos Electr* 1941;46(1):1–6.
- [42] Burton RK, McPherron R, Russell C. An empirical relationship between interplanetary conditions and *dst*. *J Geophys Res* 1975;80(31):4204–14.
- [43] Pulkkinen A, Bernabeu E, Eichner J, Beggan C, Thomson A. Generation of 100-year geomagnetically induced current scenarios. *Space Weather* 2012;10(4).
- [44] Jiang Z-Q, Zhou W-X. Multifractal analysis of Chinese stock volatilities based on the partition function approach. *Physica A* 2008;387(19–20):4881–8.